Laser-induced Structural Disordering and Optical Phase Change in Semimetal Bismuth Observed by Raman Microscopy

Ørjan S. Handegård[1,2], Masahiro Kitajima(北島正弘)[1], and Tadaaki Nagao(長尾忠昭)[1,2]

[1]*International Center for Materials Nanoarchitectonics (MANA), National Institute for Materials Science (NIMS), 1-1 Namiki, Tsukuba, Ibaraki 305-0044, Japan*

[2]*Department of Condensed Matter Physics, Hokkaido University, Kita, Sapporo, Hokkaido 060-0808, Japan*

Abstract

We observed strong enhancement of the Raman signal from a silicon (Si) substrate hidden beneath nano/micro-droplets of bismuth (Bi) after exposing them to a high-power laser beam (785 nm). Confocal Raman microscopy indicated that the as-fabricated Bi droplets inhibit the Raman signal from the underlying Si substrate. After the laser flash heating step, the intensity of Si optical phonons was strongly enhanced at the positions of Bi droplets, becoming even more intense than that of the bare Si substrate. Analyses of the Bi optical phonon modes, E_g and A_{1g}, confirmed a loss of long-range ordered crystallinity in the laser exposed droplets. Such lattice disordering can increase the available free carrier density in semimetal Bi, as occurs in the case of its amorphous and liquid states. And this can induce an optical phase change, which causes a marked enhancement of Si Raman signals through an effect similar to surface-enhanced Raman scattering (SERS).

1. Introduction

The semimetals in Group V constitute an exotic class of materials where a variety of allotropes exist depending on factors such as pressure, temperature, and their crystal growth conditions. Among these elements, bismuth (Bi) has attracted considerable interest as the prototype semimetal, showing extreme electronic, mechanical, and optical behavior, such as a huge magnetoresistance, a very low Debye temperature, and a low melting point (271 °C for bulk Bi) [1–3]. Furthermore, Bi exhibits a metal-dielectric duality in terms of its optical response and has a high refractive index in the long wavelength limit as well as plasmonic characteristics from the near-infrared to the ultraviolet spectral region [4]. These varied and unique features make this material attractive for a wide range of applications within fields, such as magnetic field sensing [5], photocatalysis [6], thermoelectric nanodevices [7], and photodetection [8]. From a structural point of view, the electronic configuration of crystalline Bi has a low free-carrier density, where conducive electrons and holes are located at tiny Fermi pockets of its band structure. When the crystallinity of semimetal Bi becomes deteriorated, the available free electron density increases owing to subtle overlap between the valence and the conduction band as in the case for amorphous Bi, which has a free electron density four-orders of magnitude higher than semimetal Bi [9]. Thus, a change in the crystal lattice of Bi can have considerable effects on its electrical- and optical conductivity. The amorphous structure of Bi has many similar features to its liquid state in terms of its electrical and optical response, and has greater metallic character [10]. The microscopic mechanism for this behavior is an intriguing subject in condensed matter physics and of technical importance for engineering applications in thermal and optoelectronic devices. Owing to the wide range of attributes and potential for future applications of Bi, there is great interest in developing methods to manipulate Bi in a controlled manner down to the nanoscale to obtain desirable properties. In order to achieve this, laser techniques offer a powerful and effective way to change material properties

and/or structural features. Lasers allow for high-level control in modifying morphologies and properties in nanofabrication approaches, where feature size is limited only by the spot size of the laser beam [11,12]. Hence, laser methods offer the ability to selectively tailor nanomaterials, and in the case of Bi, lasers can promote oxidation processes [13–15] or used to form nanoparticles by laser ablation [16]. However, studies on the effects of laser irradiation on structural, electrical, and optical properties of Bi have been lacking to date.

In this work, we report on a remarkable enhancement of the Raman signal from a silicon (Si) substrate hidden beneath Bi droplets, appearing only after exposure of Bi droplets to high-power laser irradiation. We used confocal Raman microscopy to obtain images from the Raman active Bi phonons and optical phonons of the Si. We detected a pronounced increase in the intensity of Si optical phonons beneath the Bi droplets after laser exposure and considerable changes in Bi E_g and A_{1g} modes were simultaneously detected. Additionally, spectral features in our dark-field microscopy shifted to shorter wavelengths after the laser flash heating of droplets. All together, our results suggest that an optical phase change occured due to the laser irradiation, and can be associated with an increasing metallic character in the Bi droplets, which leads to an effect similar to surface-enhanced Raman scattering (SERS) which was suggested earlier [17,18]. We discuss the correlation between the laser-induced metallicity enhancement and the plasmonic SERS effect associated with the enhanced near-field and scattering.

2. Experimental methods

The Bi droplets were fabricated from an epitaxially grown single crystal Bi(001) thin film on silicon [2,3]. Bi films with a thickness of approximately 8 nm were deposited on a reconstructed Si(111)-7×7 surface by molecular beam epitaxy (MBE) under ultra-high vacuum (UHV) at a base pressure below 10^{-9} Torr. The Bi (99.9999%, NewMet) source material was evaporated from a Knudsen effusion cell at rate of 2.5 Å/min, as monitored by a quartz crystal microbalance. The Bi droplets were prepared from the deposited film by post-annealing at roughly 300 °C, through

resistive heating of the Si substrate. The thin film deposition and resistive heating processes were monitored by *in situ* reflection high energy electron diffraction (RHEED). All the other experiments and characterization were performed at ambient temperature unless otherwise stated. A combined atomic force microscope (AFM), confocal Raman microscope, and bright-field and dark-field microscope was used for these studies (alpha300 system, WITec). We used a confocal setup for laser flash heating of our sample, together with a 785-nm diode laser (Xtra II, Toptica) operated at 30 mW. The laser spot was focused to a spot diameter of ~2 μm, with a 50× objective lens having a numerical aperture of 0.8, followed by scanning across a selected area of interest.

The morphologies of the Bi droplets before and after laser irradiation were characterized with a scanning electron microscope (SEM; SU8230, Hitachi) and AFM. The AFM topographic information was acquired in tapping mode with the use of a cantilever having a nominal resonance frequency of 75 kHz and a force constant of 2.5 N/m. Image processing, consisting of standard flattening procedures, was performed in Gwyddion [17]. For the Raman measurements, a Bragg grating coupler and a 532-nm Nd:YAG continuous wave laser source were used. The laser was focused to a spot diameter of ~1.5 μm with a 50× objective lens, and operated at a power of 6 mW. Spatially resolved Raman spectra were acquired over a 25×25 μm^2 area, with a total of 128×128 spectra and an integration time of 20 ms at each point. The spectra were optically resolved by a 1200 g/mm diffraction grating, and recorded by an Acton SP2300 spectrometer (Princeton Instruments). Phonon images were constructed by Raman peak integration with background subtraction using Project FOUR (WITec). Light scattering from the Bi droplets was characterized by reflection dark-field microscopy in a confocal configuration using a 50× objective lens and a white halogen lamp for illumination. The dark-field spectra were resolved with a 300 g/mm diffraction grating and recorded by an Acton SP2300 spectrometer.

3. Results and discussion

3.1 Formation of Bi droplets and their characterization

A schematic view of the Bi droplet fabrication process is illustrated in Fig. 1(a). The diffraction spots and streaky lines seen in the RHEED pattern (Fig. 1(b)) are characteristic of single crystalline Bi thin films with a [001] surface orientation [3,18]. Under resistive heating, the thin film integrity was disrupted and transformed from a continuous 2D film to 3D structures. This transition was monitored by observing the RHEED pattern, which changed from a characteristic 2D streaky pattern (Fig. 1(b)) to a spotted transmission pattern as 3D structures formed (Fig. 1(d)). We verified this result by SEM, comparing the as-grown thin film (Fig. 1(c)) with a post-annealed sample (Fig. 1(e)), where in the latter, the droplet shapes of Bi were clearly visible. The size distribution of the Bi droplets ranged from a few tens of nm to 2–3 μm in diameter. The resistive heating process resulted in spontaneous formation of Bi droplets on the Si surface, as is typical for thermal dewetting of a molten film with a high surface tension.

Images from a selected region of interest were captured by optical bright-field microscopy, SEM, and AFM before and after exposure to the high-power focused laser beam (785 nm), referred to here as laser flash heating. Before laser flashing, the pristine Bi droplets were smooth, hemispherical, and separately distributed throughout the substrate (Fig. 2(b), (c) and (d)). After the laser flashing step (Fig. 2(e), (f), and (g)), the appearance and morphology of the droplets changed compared with their original features. From the bright-field images, all the laser-exposed droplets appeared darker and the larger droplets widened, indicating that the scattering cross section was enhanced after the flashing (Fig. 2(b) and (e)). In the SEM images (Fig. 2(c) and (f)), the smaller droplets (< 1 μm) were less affected by laser exposure; however the height of larger droplets decreased and smaller particles appeared around them. These observations suggest that “volatile boiling” occurred during the laser flash heating step. These observations are furthermore supported by AFM results (Fig. 2(d) and (g)).

3.2 Spatially resolved optical phonons of Si

We used spatially resolved Raman microscopy to investigate any modifications to the inherent features of the system following high-power laser exposure. Raman spectra from an individual Bi droplet, under pristine and laser-flashed conditions, are shown in Fig. 3(a). To highlight the effects of the Bi droplets on the Si Raman signal (520 cm^{-1}), the signal of the bare Si substrate is subtracted from the spectra obtained from the Bi droplet. The Raman spectra (Fig. 3(a)) shows the two first-order optical phonon modes of Bi, namely the E_g (transverse) and A_{1g} (longitudinal) modes appearing at ~67 cm^{-1} and ~92 cm^{-1}, respectively. For the pristine Bi, we observed that the Raman signal from the Si substrate was much weaker at the droplet position than at the bare substrate (i.e. the peak was lower than the baseline). However, to our surprise, it increased dramatically after the laser flash heating (the Si peak become higher than the bare Si surface). These results can be seen clearly in the Raman images. For the pristine droplets (Fig. 3(b) and (d)), the intensity of the Si optical phonons was dark (low intensity) where the Bi A_{1g} was bright (high intensity). This observation indicates that the presence of Bi inhibits Raman scattering from the substrate. Conversely, for laser flashed droplets (Fig. 3(c) and (e)), the intensity of the Si optical phonons became bright where the Bi A_{1g} phonon was bright. The sharp increase in the Si Raman signal suggests that the laser flashing modulated the optical response of Bi to enhance the local electromagnetic field in proximity to the droplets, and hence the signal from the substrate. These findings will be discussed in more detail later (subsection 3.4 and 3.5).

To further connect the relationship between the optical scattering and morphology of the Bi droplets, we obtained line profiles and 3D mappings from a single micrometer-scale particle, as shown in Fig. 4. Line profiles of the Si Raman intensity, dark-field scattering intensity and AFM height measurements are given for a single droplet under pristine (Fig. 4(a)) and laser-flashed condition (Fig. 4(b)), respectively. The overlaid line profiles show good agreement between the different techniques. At the position of the Bi droplet, the Si Raman signal intensity gradually decreased towards the center of the droplet. Conversely, for the laser-flashed droplet, the Si signal intensity was greater at the droplet position, than at the bare substrate. As for the larger particles, the

Si phonon intensity did not show a uniform intensity distribution across the droplet but rather stronger enhancement was found along the edges than at the center. Interestingly, these ring-like features were observed in both Raman and dark-field results across the particle area in the 3D mappings (Fig. 4(c-e)), suggesting a common origin for this optical scattering.

To elucidate the dependence of the Si Raman signal on droplet size, the intensities of droplets of different sizes under pristine and laser flashed conditions are plotted in Fig. 5. The intensities were calculated by integrating and averaging the Si peaks over the whole droplet area for each single particle and normalized to the bare Si substrate Raman intensity. For pristine Bi droplets, the plot showed a steady decrease in the Si intensity with increasing size. Larger droplets suppressed the Si signal more completely, decreasing from approximately 0.87 to 0.12 as the size decreased from 0.5 μm to 2.7 μm, respectively. However, after laser-flashing, the Si phonon signal at the position of the Bi droplets became even greater than that of the Si substrate itself, ranging from 1.2–1.7, indicating that the irradiated Bi droplets act~~ed~~ as signal amplifiers. There is a steep increase in the relative intensity from droplets with sizes around 0.8 μm, followed by saturation at larger sizes. This steep increase is most likely associated with the change in total available free carriers in the droplet volume, which is linked with droplet size. Although the relative intensity for the laser flashed droplets saturated at 1.7, the ratio of the Si peak intensities of the laser-flashed to pristine droplets (enhancement factor) showed an almost linear increase as the droplet size increased.

3.3 Laser flash heating and lattice disordering in Bi

We adopted Raman mapping to investigate any changes in the structural properties of the Bi droplets. The scattered light detected by Raman spectroscopy gives information about a material's vibrational modes, and details concerning the crystal phase, stress, and structural point defects can be obtained. We examined the intensities and linewidths of the Bi optical phonon modes in the Raman spectra, and can discuss the changes of crystallinity and local atomic rearrangement caused

by the laser-flashed heating. Micro-Raman spectra obtained from a representative Bi droplet, for pristine and laser-flashed condition, are given in Fig. 6(a). As previously mentioned, the E_g and A_{1g} modes of rhombohedral Bi were detected at 67 cm^{-1} and at 92 cm^{-1}, respectively. The two-fold degenerate E_g transverse optical mode is produced by atomic displacement occurring within the plane of the Bi interlayer (parallel with the (001) plane). The displacement of the symmetric A_{1g} longitudinal mode occurs in between the bilayers (perpendicular to the (001) plane), as shown in Fig. 6(b) and (c). The sharp Raman peaks of the E_g and A_{1g} modes indicate that the pristine droplets were highly crystalline, and the E_g signal was approximately twice as intense as the A_{1g} signal (Fig. 6(a)). After high-power laser irradiation, the E_g and A_{1g} signals exhibited a comparable intensity and their peak width broadened considerably. Because of the sensitivity of Raman spectroscopy to crystallinity, these peak changes indicate a change in the preferential structure orientation of the laser flashed droplets compared with the pristine droplets. The relative peak intensity between optical phonon modes is useful as an indicator for studying disorder and phase changes, and has been frequently used for determining defects in and phase of carbon materials and others [19,20]. For example, Raman peak broadening in Bi correlate with crystal point defects, as has previously been shown for the A_{1g} mode where the vibrational decay rate/damping increases as more defects are introduced [21]. For our Raman spectra, by applying Lorentzian peak fitting to the observable Bi phonon modes, we measured full-width at half-maximum (FWHM) broadening from 14.2 to 25.6 cm^{-1} and a frequency shift from 66.7 to 68.1 cm^{-1} for the E_g mode. For the A_{1g} mode, we observed a FWHM broadening from 13.1 to 24.8 cm^{-1} and a frequency shift from 92.6 to 91.8 cm^{-1}. The intensity ratio of E_g/A_{1g} decreased from 2.07 to 0.99. The peak shifts, broadening, and E_g/A_{1g} intensity ratio change for the laser flashed Bi droplets suggest: 1) deterioration of long-range order by defect formation; and 2) changes in the local bonding character or atomic remodeling, caused by the high-power laser irradiation. Most likely, the laser-flash heating transformed the crystalline Bi microdroplets into a more amorphous- or liquid-like state, which can increase the metallic character of Bi, as has been previously reported [9,10] and is inferred above. Another observation from the

Raman spectra of the laser irradiated droplets is the appearance of two new peaks, indicating the formation of bismuth oxide (Bi_2O_3). Many phases of Bi_2O_3 exist, however, only the β-Bi_2O_3 phase was reported to form through laser flashing, which was confirmed by the peak positions at 125 and 314 cm^{-1} characteristic of β-Bi_2O_3 [14,15]. According to preceding work, the onset of β-Bi_2O_3 formation under ambient conditions takes place only above the melting point of Bi [14]. The presence of Bi oxide peaks thus confirmed that Bi droplets underwent local melting and resolidification induced by the laser flashing step. This rapid resolidification distorts the pristine Bi lattice, as observed from the changes in optical phonon modes of Bi.

3.4 Optical phase change in Bi and Si Raman signal enhancement

To further investigate the correlation between the structural transition in Bi droplets and observed strong Raman signal enhancement of Si, we collected dark-field microscopy spectra and constructed spectral images from scattered white light by pristine and laser flashed Bi droplets, as shown in Fig. 7. The dark-field spectra exhibited clear feature in the visible to the near infrared region, and their peak positions shift to lower wavelengths after the laser-flashing of Bi droplets (Fig. 7(a)). We attribute this spectral blue shifts to lower wavelengths to an increase in the free carrier concentration, as well as size and shape effects. Because the morphology was not markedly changed after laser flashing, based on AFM and SEM observations, a change in the available carrier density would be the most possible contributing factor to the altered scattering properties of the laser flashed Bi droplets. As for the bright-field images shown in Fig. 2, the droplets in the dark-field images (Fig. 7(b) and (c)) became darker after laser flashing, also indicative of a modulation of the scattering properties.

On the basis of the present results, we discuss the origin of the Si Raman signal enhancement by Bi droplets on the Si substrate. A previous study by Hunderi on the optical properties of Bi reported that in its amorphous state, Bi has properties similar to its liquid state, i.e., a higher density of available carriers and its optical properties that are well described by the Drude

model [9]. Similarly, a more recent study has shown that at the transition from solid to liquid phase, the real part of the dielectric function (ε_1) becomes more negative and the imaginary part (ε_2) increases [10], which is a characteristic of a Drude metals. In the case of disordered Bi, it is expected that it becomes more metallic in nature as its amorphousness increases. When the crystalline structure of semimetal Bi becomes distorted, subtle overlap between the valence and conduction band occurs, leading to a sharp increase in metallic character and an altered electrical and optical response. In other words, the absorption coefficient and refractive index of Bi are strongly influenced by the state of its crystal lattice. These arguments can consistently explain our findings, where in the Raman spectra we detected a lattice disorder in Bi, strong enhancement in Si phonons beneath the Bi droplets, as well as blueshifts in dark-field scattering spectra, which all occuring only after the laser flash heating step. Especially, the strong enhancenet of Si Raman signal at the position of Bi droplets strongly suggests an optical phase change occurring in Bi [9,10,22,23]. The local heating and subsequent melting of Bi droplets, induced by the high-power laser irradiation, are followed by rapid cooling through the Si substrate, which has high thermal conductivity to dissipate the heat. Under these conditions the Bi droplets resolidify with a low degree of crystallinity. Thus, the laser flashed Bi droplets is transformed into a state with properties closer to those of liquid or amorphous Bi, which have metallic rather than semimetallic characteristics.

Our observations of the optical phase change are possibly related to surface enhanced Raman scattering (SERS) effects, which arises from an increase in free available carriers in the disordered Bi [9,18]. Compared to the pristine Bi droplets, laser flashing introduces lattice disorder which relax from an open-packed covalent-like lattice to a more close-packed metal-like lattice driving it to a more conductive state. Thus disordering thrusts the dielectric function of Bi converted to a more plasmonic one, leading to stronger light scattering as well as local near-field enhancements compared to the pristine case. Therefore laser induced phase chage makes the Bi droplets exhibit dramatic change in bright/dark-field micrographs, spectral blue shifts, and the

pronounced SERS-like behavioirs as observed in this study. Such phase change phenomena in optical properties are an interesting topic for future studies in terms of fundamental science and for potential device applications. The melting and quench cooling of nano-/microscale objects, such as Bi in the current study, will open a new route to tuning the optical/electrical functionality of nanosystems and expand the range of studies in materials science and nanotechnology.

4. Conclusions

We prepared well-defined Bi droplets on a Si(111) substrate by thermal dewetting of an epitaxially grown Bi thin film. We demonstrated that the Bi droplets show a large change in their optical response after laser flashing, as visualized by Raman microscopy. After laser flashing, the Si Raman signals increased markedly at Bi droplet locations. The drastic change in Raman spectra indicate that the droplets underwent an optical phase change from inhibiting to enhancing the Raman signal intensity of underlying Si substrate. The white light scattering spectra of Bi droplets, collected by dark-field microscopy, exhibited systematic spectral shifts towards shorter wavelengths after laser exposure. These observations clearly indicate a change in the optical response of Bi, as it shifted to a highly metallic phase, exhibiting a SERS-like effect. We propose that this transition in the optical phase arises because of lattice distortions, introduced by melting and quench-cooling by laser flashing, which influence the available carrier concentration of Bi. Our study demonstrates the potential for tailoring the optical response of nano/micro-scale objects by laser irradiation, which might open new paths of exploration in controlling the optical functionalities of materials.

Acknowledgements

This work is partially supported by JSPS KAKENHI (16F16315, JP16H06364, 16H03820), and CREST "Phase Interface Science for Highly Efficient Energy Utilization" (JPMJCR13C3) from

Japan Science and Technology Agency. We are also thankful to S. Ishii, T. D. Dao, and H. D. Ngo for fruitful discussions.

References

[1] Y. Fuseya, M. Ogata, H. Fukuyama, Transport properties and diamagnetism of dirac electrons in bismuth, J. Phys. Soc. Japan. 84 (2015) 54–56. doi:10.7566/JPSJ.84.012001.

[2] T. Nagao, J.T. Sadowski, M. Saito, S. Yaginuma, Y. Fujikawa, T. Kogure, T. Ohno, Y. Hasegawa, S. Hasegawa, T. Sakurai, Nanofilm allotrope and phase transformation of ultrathin Bi film on Si(111)-7×7, Phys. Rev. Lett. 93 (2004) 10–13. doi:10.1103/PhysRevLett.93.105501.

[3] S. Yaginuma, T. Nagao, J.T. Sadowski, M. Saito, K. Nagaoka, Y. Fujikawa, T. Sakurai, T. Nakayama, Origin of flat morphology and high crystallinity of ultrathin bismuth films, Surf. Sci. 601 (2007) 3593–3600. doi:10.1016/j.susc.2007.06.075.

[4] J. Toudert, R. Serna, I. Camps, J. Wojcik, P. Mascher, E. Rebollar, T.A. Ezquerra, Unveiling the Far Infrared-to-Ultraviolet Optical Properties of Bismuth for Applications in Plasmonics and Nanophotonics, J. Phys. Chem. C. 121 (2017) 3511–3521. doi:10.1021/acs.jpcc.6b10331.

[5] K. Liu, P. Searson, F.Y. Yang, K. Liu, K. Hong, D.H. Reich, P.C. Searson, Yang , F . Y . et al . Large magnetoresistance of electrodeposited single-crystal bismuth thin Large Magnetoresistance of Electrodeposited Single-Crystal Bismuth Thin Films, 284 (1999) 1335–1337. doi:10.1126/science.284.5418.1335.

[6] F. Dong, Z. Zhao, Y. Sun, Y. Zhang, S. Yan, Z. Wu, An Advanced Semimetal-Organic Bi Spheres-g-C3N4Nanohybrid with SPR-Enhanced Visible-Light Photocatalytic Performance for NO Purification, Environ. Sci. Technol. 49 (2015) 12432–12440. doi:10.1021/acs.est.5b03758.

[7] M.S. Dresselhaus, Y.M. Lin, O. Rabin, A. Jorio, A.G. Souza Filho, M.A. Pimenta, R. Saito, G. Samsonidze, G. Dresselhaus, Nanowires and nanotubes, Mater. Sci. Eng. C. 23 (2003) 129–140. doi:10.1016/S0928-4931(02)00240-0.

[8] J.D. Yao, J.M. Shao, G.W. Yang, Ultra-broadband and high-responsive photodetectors based on bismuth film at room temperature, Sci. Rep. 5 (2015) 1–7. doi:10.1038/srep12320.

[9] O. Hunderi, Optical properties of crystalline and amorphous bismuth films, J. Phys. F Met. Phys. 5 (1975) 2214–2225.

[10] L. Yang, Y.X. Zheng, S.D. Yang, Z.H. Liu, J.B. Zhang, R.J. Zhang, S.Y. Wang, D.X. Zhang, L.Y. Chen, Ellipsometric study on temperature dependent optical properties of topological bismuth film, Appl. Surf. Sci. 421 (2017) 899–904. doi:10.1016/j.apsusc.2016.11.006.

[11] K.C. Phillips, H.H. Gandhi, E. Mazur, S.K. Sundaram, Ultrafast laser processing of materials: a review, Adv. Opt. Photonics. 7 (2015) 684–712.

[12] M. Malinauskas, A. Žukauskas, S. Hasegawa, Y. Hayasaki, V. Mizeikis, R. Buividas, S. Juodkazis, Ultrafast laser processing of materials: from science to industry, Light Sci. Appl. 5 (2016) e16133. doi:10.1038/lsa.2016.133.

[13] L. Kumari, J.H. Lin, Y.R. Ma, Laser oxidation and wide-band photoluminescence of thermal evaporated bismuth thin films, J. Phys. D. Appl. Phys. 41 (2008). doi:10.1088/0022-3727/41/2/025405.

[14] J.A. Steele, R.A. Lewis, Laser-induced oxidation kinetics of bismuth surface microdroplets on GaAsBi studied in situ by Raman microprobe analysis, Opt. Express. 22 (2014) 32261. doi:10.1364/OE.22.032261.

[15] C. Díaz-Guerra, P. Almodóvar, M. Camacho-López, S. Camacho-López, J. Piqueras, Formation of β-Bi2O3and δ-Bi2O3during laser irradiation of Bi films studied in-situ by spatially resolved Raman spectroscopy, J. Alloys Compd. 723 (2017) 520–526. doi:10.1016/j.jallcom.2017.06.263.

[16] S. Onari, M. Miura, K. Matsuishi, Raman spectroscopic studies on bismuth nanoparticles prepared by laser ablation technique, Appl. Surf. Sci. 197–198 (2002) 615–618. doi:10.1016/S0169-4332(02)00410-5.

[17] A.G. Bezerra, P. Cavassin, T.N. Machado, T.D. Woiski, R. Caetano, W.H. Schreiner, Surface-enhanced Raman scattering using bismuth nanoparticles: a study with amino acids, J. Nanoparticle Res. 19 (2017). doi:10.1007/s11051-017-4057-6.

[18] J. Toudert, R. Serna, M. Jiménez De Castro, Exploring the optical potential of nano-bismuth: Tunable surface plasmon resonances in the near ultraviolet-to-near infrared range, J. Phys. Chem. C. 116 (2012) 20530–20539. doi:10.1021/jp3065882.

[19] D. Nečas, P. Klapetek, Gwyddion: An open-source software for SPM data analysis, Cent. Eur. J. Phys. 10 (2012) 181–188. doi:10.2478/s11534-011-0096-2.

[20] K. Yokota, J. Takeda, C. Dang, G. Han, D.N. McCarthy, T. Nagao, S. Hishita, M. Kitajima, I. Katayama, Surface metallic states in ultrathin Bi(001) films studied with terahertz time-domain spectroscopy, Appl. Phys. Lett. 100 (2012). doi:10.1063/1.4729149.

[21] M.A. Pimenta, G. Dresselhaus, M.S. Dresselhaus, L.G. Cançado, A. Jorio, R. Saito, Studying disorder in graphite-based systems by Raman spectroscopy, Phys. Chem. Chem. Phys. (2007). doi:10.1039/b613962k.

[22] P. Colomban, A. Slodczyk, Raman intensity: An important tool in the study of nanomaterials and nanostructures, Acta Phys. Pol. A. 116 (2009) 7–12. doi:10.12693/APhysPolA.116.7.

[23] M. Hase, K. Ishioka, M. Kitajima, K. Ushida, S. Hishita, Dephasing of coherent phonons by lattice defects in bismuth films, Appl. Phys. Lett. 76 (2000) 1258–1260. doi:10.1063/1.126002.

[24] K.J. Miller, R.F. Haglund, S.M. Weiss, Optical phase change materials in integrated silicon photonic devices: review, Opt. Mater. Express. (2018). doi:10.2337/db07-1472.

[25] S. Raoux, Phase Change Materials, Annu. Rev. Mater. Res. 39 (2009) 25–48. doi:10.1146/annurev-matsci-082908-145405.

[26] P. Cucka, C.S. Barrett, The crystal structure of Bi and of solid solutions of Pb, Sn, Sb and Te in Bi, Acta Crystallogr. 15 (1962) 865–872. doi:10.1107/S0365110X62002297.

[27] F. Momma, K. and Izumi, VESTA 3 for three-dimensional visualization of crystal, volumetric and morphology data, J. Appl. Crystallogr. 44 (2011) 1272–1276.

Figure captions

Fig. 1. (a) Schematic diagram of Bi droplet preparation by thermal dewetting of Bi thin film. RHEED patterns were recorded (b) before and (d) after resistive heating of Si substrate. (c) A SEM image of an as-grown Bi film with a 0.5μm scale bar. (e) A SEM image of the pristine Bi droplets with a 1μm scale bar.

Fig. 2. (a) Schematic illustration of the laser irradiation process of Bi droplets. Droplets were characterized before and after high-power laser exposure, respectively, by (b) and (e) an optical bright field microscope, (c) and (f) SEM, and (d) and (g) AFM imaging. Scale bars in all images are 5 μm. Insets in (c) and (f) show close-up SEM images tilted at 45°, with a 1-μm scale bar.

Fig. 3. (a) Micro-Raman spectra of a single Bi droplet in pristine (blue) and after laser flashing (red). Background signal from Si substrate (I_{si}) has been subtracted from the Raman spectra. Spectrum from pristine droplet has been offset. 2D images of Bi A_{1g} and Si phonon integrated

intensities across a single Bi droplet are also shown as insets. Raman mapping images constructed by integration of the Bi A_{1g} and Si peaks for (b),(c) pristine and (d),(e) laser-flashed droplets, respectively. Scale bars in Raman images are 5 μm.

Fig. 4. Raman, dark-field, and AFM line profiles, from a single Bi droplet, (a) for pristine and (b) for laser-flashed conditions. Corresponding 3D maps of the Bi droplet are shown, in (c) for Raman Si intensity, (d) for dark-field intensity, and (e) for AFM topography, before and after laser flashing. AFM height color scale bar ranges from 0 to 1 μm. The dotted horizontal lines in (a) and (b) indicates the Si Raman peak intensity of the bare Si substrate.

Fig. 5. Si Raman peak intensities at Bi droplets positions plotted as a function of droplet size for pristine (blue) and laser-flashed (red) droplets. The Si intensities are obtained by averaging across droplet area and are normalized to the Si substrate intensity (calculated as $Intensity_{Si}$ at the droplets divided by $Intensity^*_{Si}$ for the substrate). Inset shows the enhancement, calculated as the ratio of the Si intensity for the same individual particles before and after irradiation as a function of Bi droplet size (ratio between the blue and the red plots).

Fig. 6. (a) Raman spectra of an individual Bi droplet showing the E_g and A_{1g} modes. The E_g and A_{1g} peaks are fitted with a Lorentzian curve (dashed line). The peak located at 125 cm^{-1} belongs to β-Bi_2O_3. Change in the intensity ratio, peak broadening, and increased background is clearly seen. (b) The rhombohedral unit cell of Bi is shown within a hexagonal framework, where the displacement vectors for E_g and A_{1g} modes are given for two atoms. Red surface indicates the (001) plane. Atoms outside of the rhombohedral cell are omitted. (c) Side view along the x-axis of a slice from the Bi crystal showing its bilayer stacking along the z-axis. E_g displacement occurs within bilayer plane whereas A_{1g} displacement is normal to the bilayer. Crystal structure parameters of Bi were used from [24] and imported to VESTA [25].

Fig. 7. Dark-field scattering spectra from three Bi droplets are given in (a). Dark-field images before and after laser exposure are shown in (b) and (c), taken from the same area. The spectra in (a) are taken from, pristine (I, II, III) and laser flashed (I*, II* and III*) droplets as shown in (b) and (c), respectively.

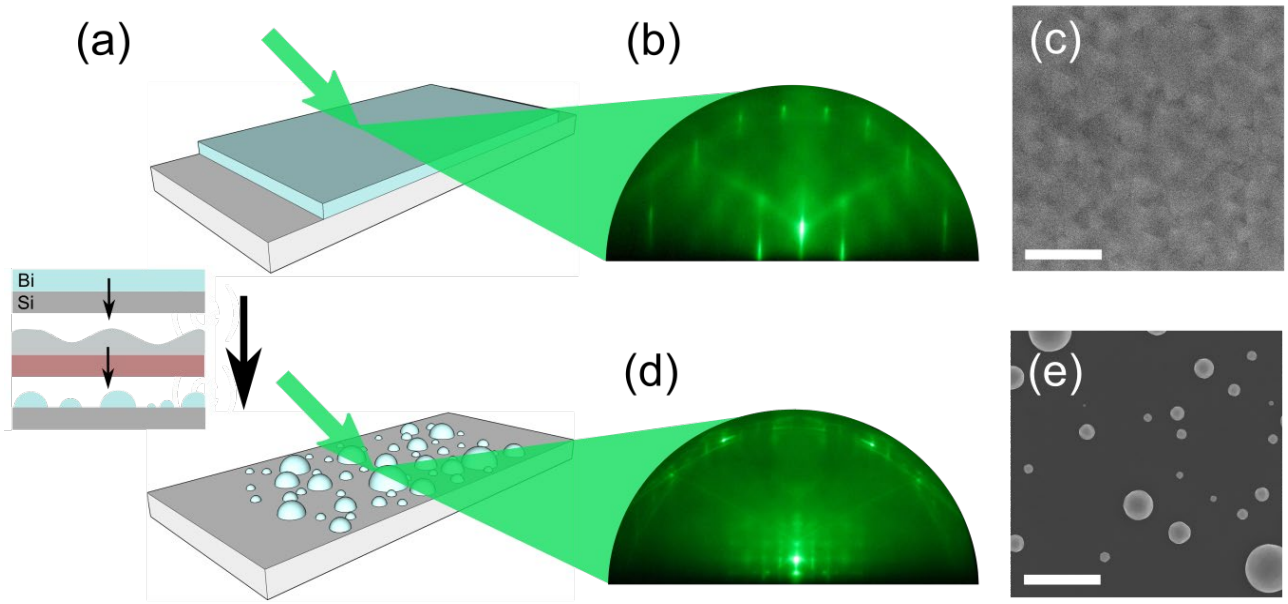

Fig. 1. (colour) Ø. S. Handegård et al.

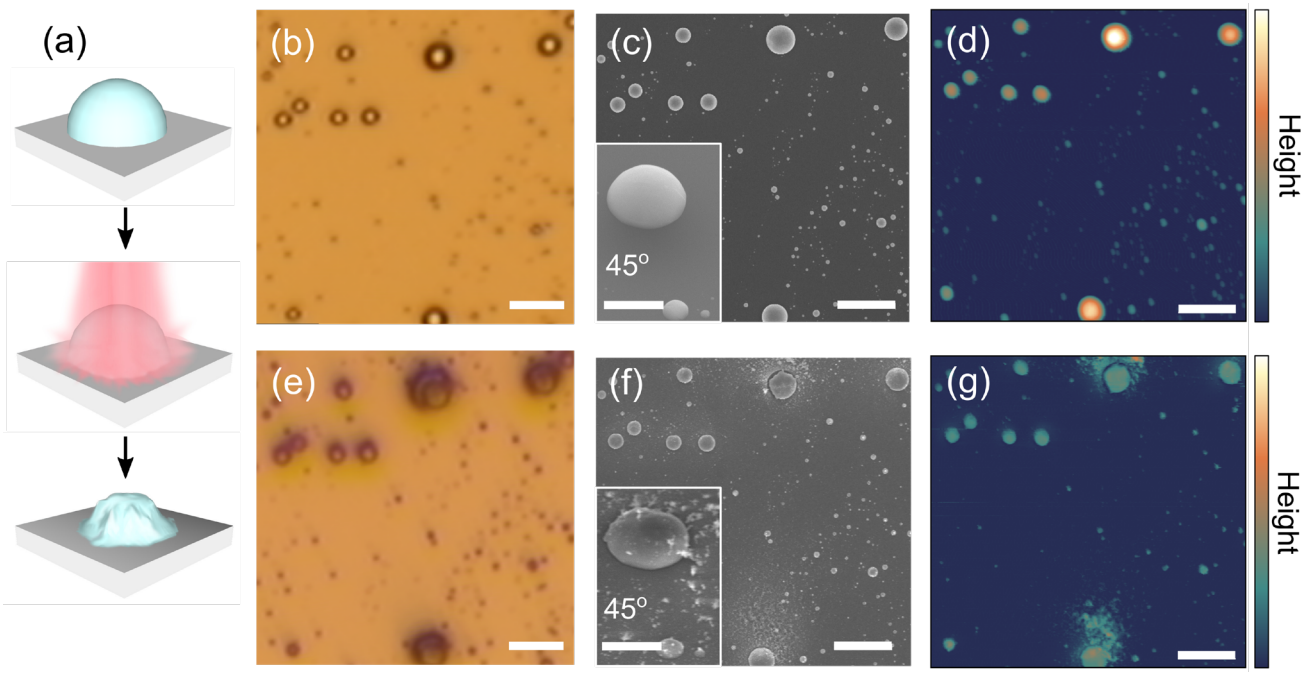

Fig. 2. (colour) Ø. S. Handegård et al.

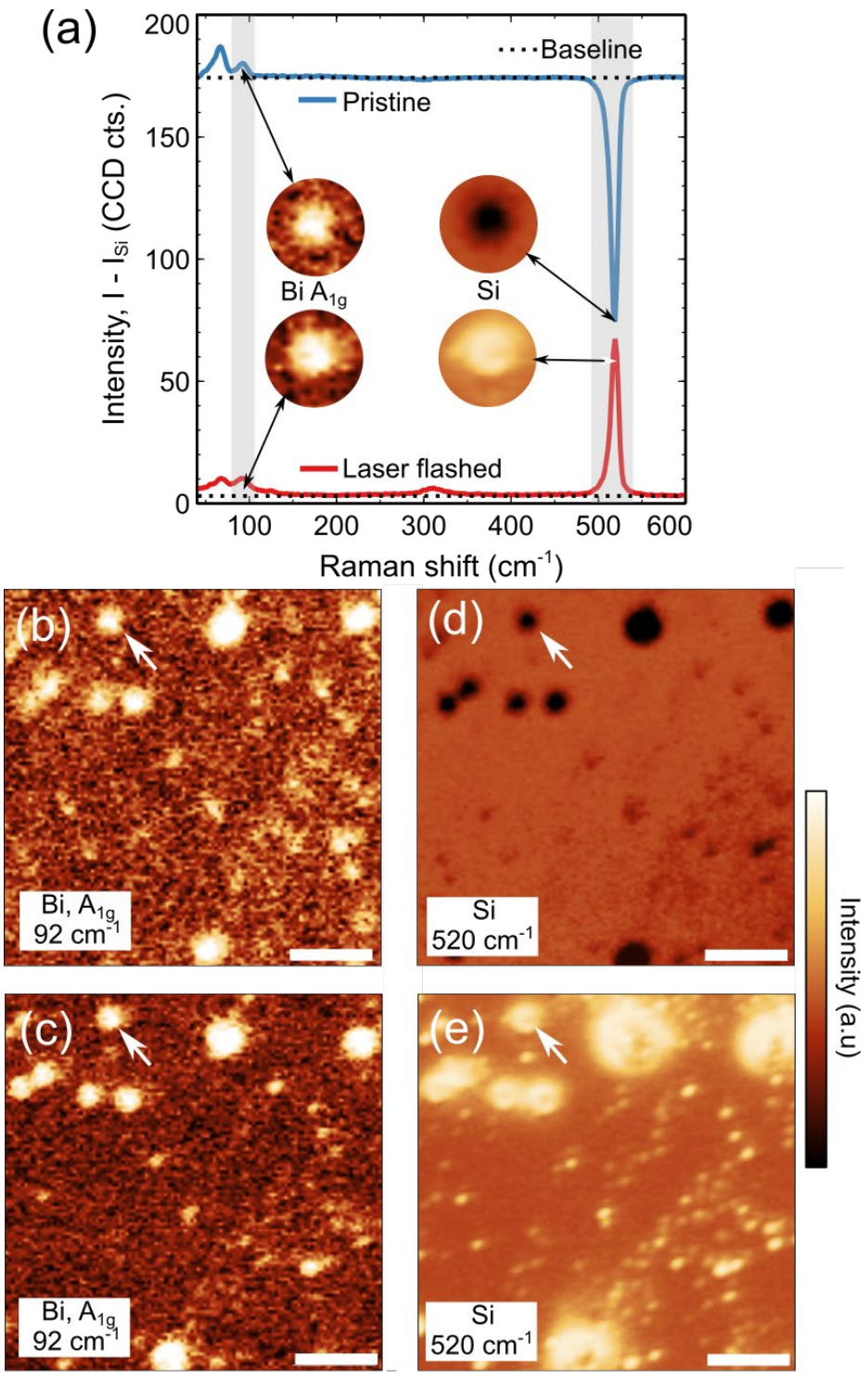

Fig. 3. (colour) Ø. S. Handegård *et al.*

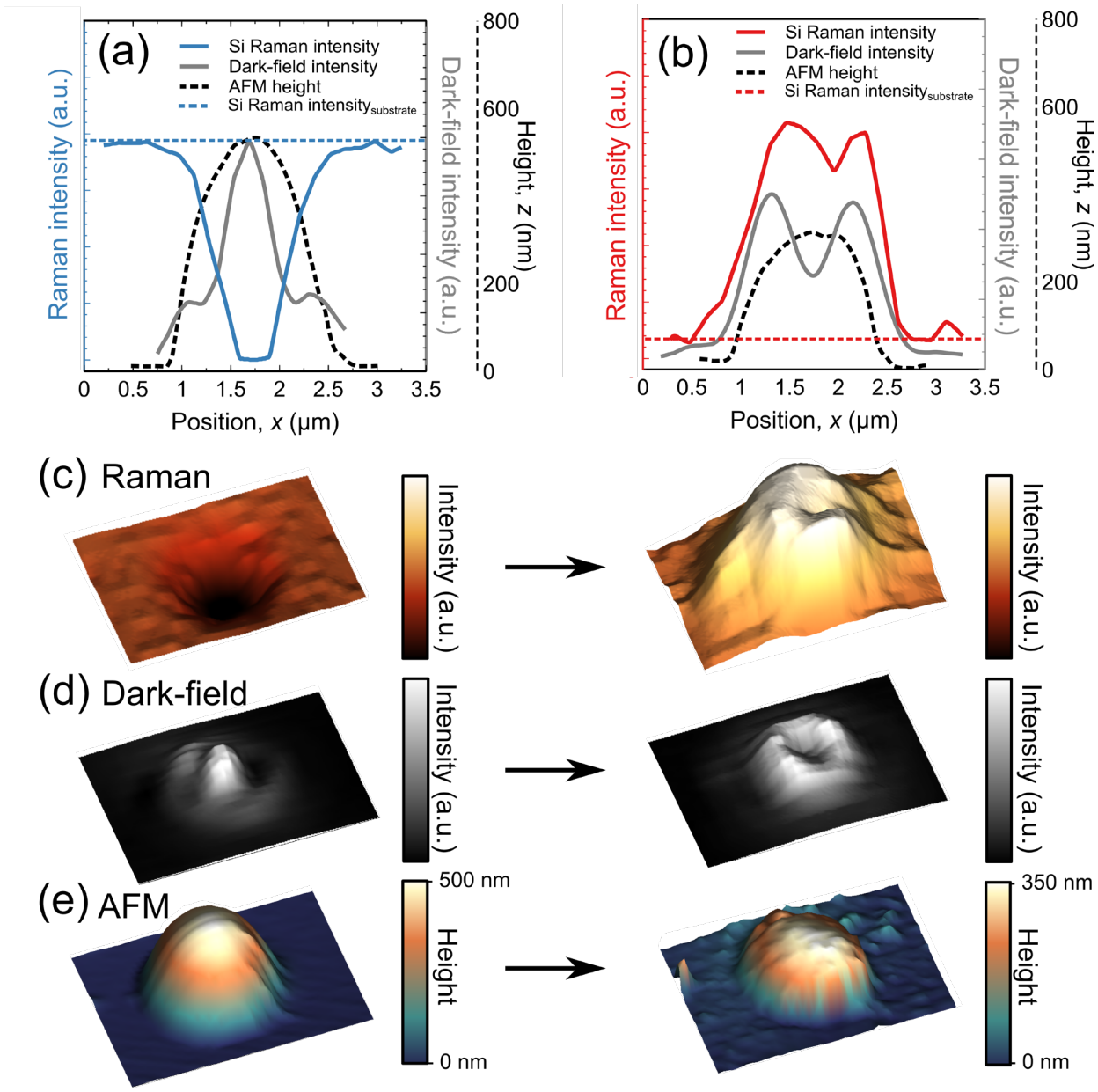

Fig. 4. (colour) Ø. S. Handegård *et al.*

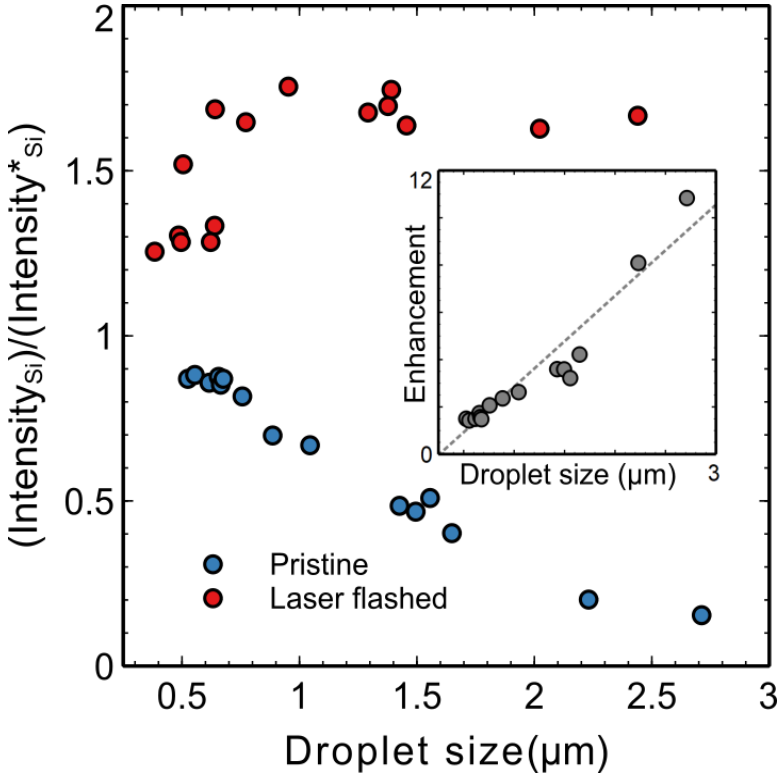

Fig. 5. (colour) Ø. S. Handegård *et al.*

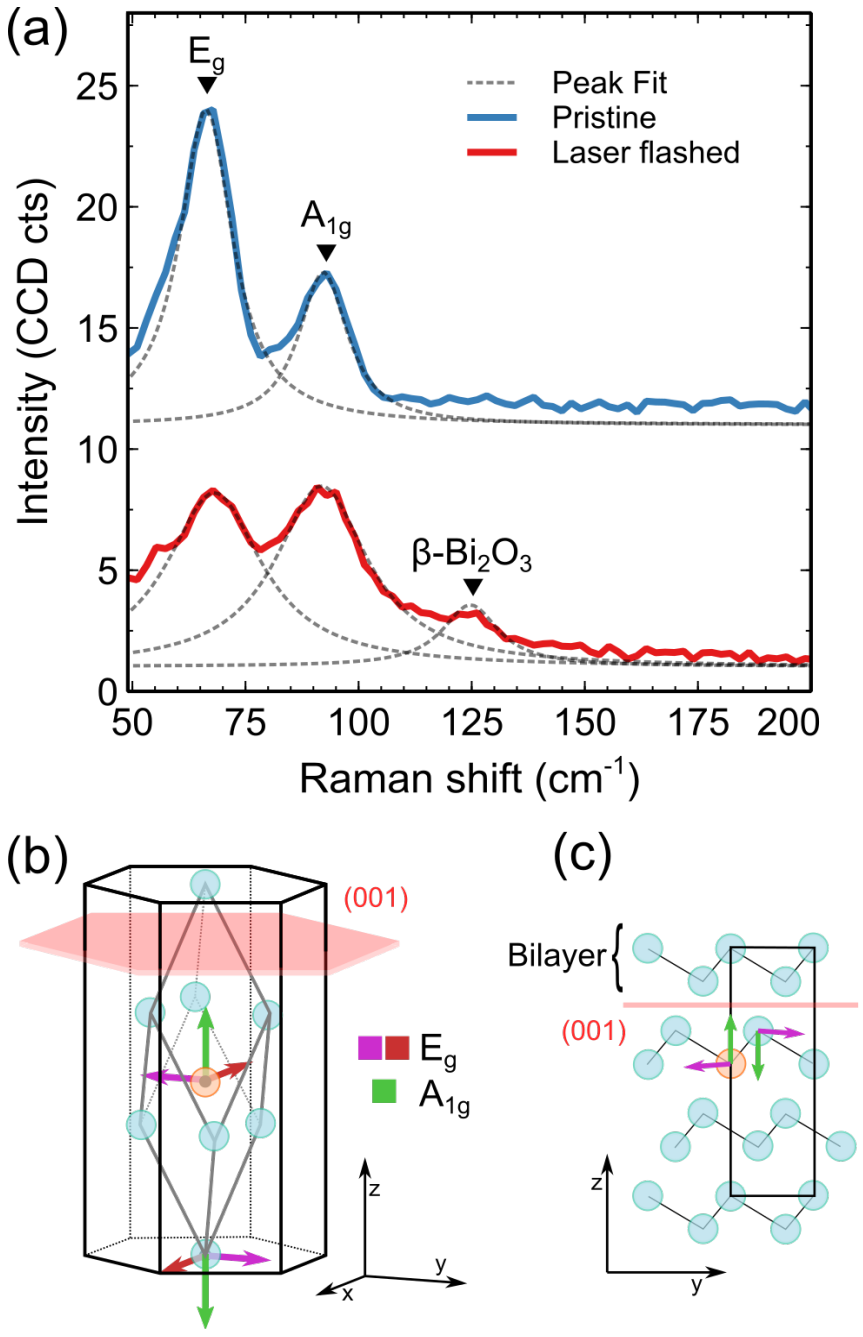

Fig. 6. (colour) Ø. S. Handegård *et al.*

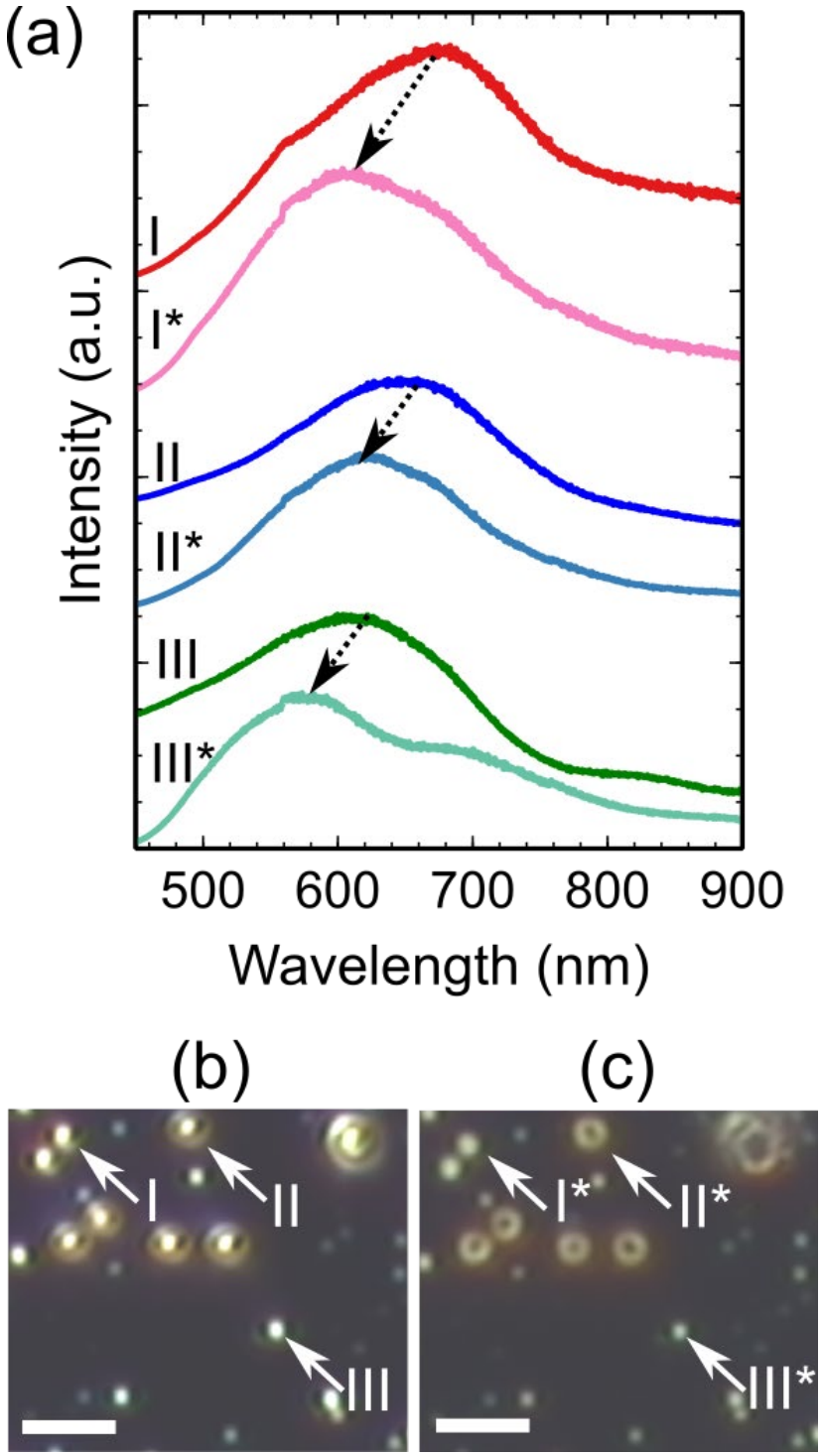

Fig. 7. (colour) Ø. S. Handegård *et al.*